Multi-site co-mutations and 5'UTR CpG immunity escape drive the evolution of SARS-CoV-2

Jingsong Zhang[1], Junyan Kang[2,3], Mofang Liu[2,3], Benhao Han[1], Li Li[4], Yongqun He[5], Zhigang Yi[6,7]*, Luonan Chen[1,8,9,10]*

[1]Key Laboratory of Systems Biology, State Key Laboratory of Cell Biology, Shanghai Institute of Biochemistry and Cell Biology, Center for Excellence in Molecular Cell Science, Chinese Academy of Sciences, Shanghai 200031, China

[2]State Key Laboratory of Molecular Biology, Shanghai Key Laboratory of Molecular Andrology, Shanghai Institute of Biochemistry and Cell Biology, Center for Excellence in Molecular Cell Science, Chinese Academy of Sciences, Shanghai 200031, China

[3]University of Chinese Academy of Sciences, Shanghai 200031, China

[4]Department of Genetics, Harvard Medical School, Boston, MA 02115, USA

[5]University of Michigan Medical School, Ann Arbor, MI 48109, USA

[6]Shanghai Public Health Clinical Center, Fudan University, Shanghai 201508, China

[7]Key Laboratory of Medical Molecular Virology (MOE/NHC/CAMS), School of Basic Medical Sciences, Shanghai Medical College, Fudan University, Shanghai 200032, China

[8]School of Life Science and Technology, ShanghaiTech University, Shanghai 201210, China.

[9]Key Laboratory of Systems Biology, Hangzhou Institute for Advanced Study, University of Chinese Academy of Sciences, Hangzhou 310024, China

[10]Center for Excellence in Animal Evolution and Genetics, Chinese Academy of Sciences, Kunming 650223, China.

*Corresponding author: Email: lnchen@sibs.ac.cn(L.N.C.); zgyi@fudan.edu.cn(Z.G.Y.)

ABSTRACT

The SARS-CoV-2 infected cases and the caused mortalities have been surging since the COVID-19 pandemic. Viral mutations emerge during the virus circulating in the population, which is shaping the viral infectivity and pathogenicity. Here we extensively analyzed 6698 SARS-CoV-2 whole genome sequences with specific sample collection dates in NCBI database. We found that four mutations, i.e., 5'UTR_c-241-t, NSP3_c-3037-t, NSP12_c-14408-t, and S_a-23403-g, became the dominant variants and each of them represented nearly 100% of all virus sequences since the middle May, 2020. Notably, we found that co-occurrence rates of three significant multi-site co-mutational patterns, i.e., (i) S_a-23403-g, NSP12_c-14408-t, 5'UTR_c-241-t, NSP3_c-3037-t, and ORF3a_c-25563-t; (ii) ORF8_t-28144-c, NSP4_c-8782-t, NSP14_c-18060-t, NSP13_a-17858-g, and NSP13_c-17747-t; and (iii) N_g-28881-a, N_g-28882-a, and N_g-28883-c, reached 66%, 90%, and nearly 100% of recent sequences, respectively. Moreover, we found significant decrease of CpG dinucleotide at positions 241(c)-242(g) in the 5'UTR during the evolution, which was verified as a potential target of human zinc finger antiviral protein (ZAP). The four dominant mutations, three significant multi-site co-mutations, and the potential escape mutation of ZAP-target in 5'UTR region contribute to the rapid evolution of SARS-CoV-2 virus in the population, thus shaping the viral infectivity and pathogenicity. This study provides valuable clues and frameworks to dissect the viral replication and virus-host interactions for designing effective therapeutics.

INTRODUCTION

Since the outbreak of COVID-19 in December 2019, it has been pandemic in over 200 countries. The infected cases and the mortalities have been surging, which is an ongoing threat to the public health (*1, 2*). COVID-19 is caused by infection with a novel coronavirus SARS-CoV-2 (*3-5*). Even though as a coronavirus, SARS-CoV-2 has genetic proofreading mechanisms (*6-8*), the persistent natural selective pressure in the population drives the virus to gradually accumulate favorable mutations (*6, 9*). Considerable attention is given to the mutation and evolution of SARS-CoV-2, for that viral mutations have important impact on the infection and pathogenicity of viruses (*10*). The beneficial mutants can better evolve and adapt to host (*9*), either strengthening or weakening the infectivity and pathogenicity. In addition, the variants may generate drug resistance and shrink the efficacy of vaccine and therapeutics (*11, 12*). Dissecting the evolutional trajectory of the virus in the

population provides important clues to understand the viral replication and virus-host interactions and helps designing effective therapeutics.

In this study, we used a NCBI dataset consisting of 6698 high-quality SARS-CoV-2 whole genome sequences with sample collection dates ranging from Dec. 20, 2019 to Jun. 8, 2020. By extensive sequence analysis, we identified the significant and convergent features of the accumulated viral mutations and CpG variations over time. Specifically, in the 29903nt viral genome, four significant mutations, i.e., 5'UTR_c-241-t, NSP3_c-3037-t, NSP12_ c-14408-t, and S_ a-23403-g, were found to become the dominant variants since early March, 2020, and each of them reached almost 100% of all virus sequences. By global statistical analyzing, we identified 14 mutation sites with significant high rates. In addition, we evaluated the mutation trajectories by each day and every 10 days, and notably identified three co-mutation patterns consisting of these 13 sites (among these 14 sites) with surprisingly high co-occurrence rates. Moreover, we found the significant decrease of CpG dinucleotides in the viral genome over time, suggesting an evolutional escape of host innate immunity of CpG (*13-15*). The dissected evolution trajectory that the four dominant mutations, three significant multi-site co-mutations, and CpG (decrease) mutation contribute to the rapid evolution of SARS-CoV-2 virus in the population, which shapes the viral infectivity and pathogenicity. This study provides valuable clues and frameworks to dissect the viral replication and virus-host interactions for designing effective therapeutics.

RESULTS

Dominant mutations appeared in SARS-CoV-2 in COVID-19 population over time

To explore the mutational landscape of SARS-CoV-2 during virus circulating in the COVID-19 population since the outbreak of COVID-19, we aligned 6698 high quality full-length genome sequences across all major regions with viral sample collection dates ranging from Dec. 20, 2019 to Jun. 8, 2020. As the mutation landscape was massive up to date, we identified 82 mutation sites with mutation rate >1% to draw a heatmap (Fig. 1A). As shown in Fig. 1, the Y-axis represents the collection dates of COVID-19 samples, each of which contains 1~225 sequences. According to the first posted viral sequence (NC_045512), there were accumulated mutations during the virus circulating and apparently new mutation sites gradually emerged since the end of Feb. 2020. Noted that several highly mutated sites appeared before Feb. 22, 2020, which was likely due to the limited collected sequences available at that time and accidental random mutations, i.e., a high mutation rate resulted from even one mutation site. Up to now, there were at least four dominant mutations

(5'UTR_c-241-t, NSP3_c-3037-t, NSP12_c-14408-t, and S_a-23403-g) (Fig. 1A), where S_ a-23403-g mutation resulted in the amino acid change (D614G) that enhances viral infectivity (*6, 16*), albeit debate exists (*10*). In particular, each of them covered almost 100% of all virus sequences since the middle May 2020. Focusing on eight mutation sites (5'UTR_c-241-t, NSP3_c-3037-t, NSP12_ c-14408-t, S_a-23403-g, ORF3a_g-25563-t, N_ g-28881-a, N_ g-28882-a, and N_g-28883-c), all the sites sites began to have very high mutation rates since May 2020 (Fig. 1B to 1F). Notably, mutations in three adjacent sites in N (N_g-28881-a, N_g-28882-a, and N_g-28883-c) co-occurred (Fig. 1G-I), suggesting a strong selection pressure.

Strong co-occurrent mutations appeared on multiple sites over time

We assessed the mutations of all residues of the SARS-CoV-2 based on the collected genome sequences. The top 34 mutation sites (with mutation rate>2%) were listed in Fig. 2A. Clearly, there were four dominant mutants (S_a-23403-g, NSP12_c-14408-t, 5'UTR_c-241-t, and NSP3_c-3037-t). The three adjacent sites in Nucleocapsid (N) also had considerably high mutation rates (>0.08). By analyzing the top 34 mutations, there were biased mutation patterns, e.g. the ratio of c-to-t (c-t) was more than 44% (Fig. 2B). We then studied the global co-occurrence relationships of the 34 mutations. We found that there were strong co-occurrence site pairs/associations (Fig. 2C) such as the following three multi-site patterns (i) S_a-23403-g, NSP12_c-14408-t, 5'UTR_c-241-t, NSP3_c-3037-t, ORF3a_c-25563-t, and ORF3a_g-25563-t; (ii) ORF8_t-28144-c, NSP4_c-8782-t, NSP14_c-18060-t, NSP13_a-17858-g, and NSP13_c-17747-t; and (iii) N_g-28881-a, N_g-28882-a, and N_g-28883-c. We further quantified the co-occurrence significance (the ratio of co-occurrence mutants to all sequence examples, also called Support (*17-19*) in data mining) among the top 11 mutation sites (mutation rate>10%) (Fig. 2E to 2I). The Y-axes represented the co-occurrence site pairs. For simplicity, we used gene names instead of their mutation sites in Fig. 2E to 2I. The corresponding mutational positions of genes were given in Fig. 2E in details. From Fig. 2F, every mutational association was significant (>0.10) in all collected genome sequences and almost all associations (except NSP4-NSP13a pair) met strong co-occurrence relationships (>0.60). Figs. 2H-2J show 3-to-6 mutation-site (multi-site) co-occurrences. Interestingly, all mutational associations in Fig. 2H to 2J follow significant and strong co-occurrence relationships. The significant co-occurrences of multi-site mutations may suggest that these sites closely interact with each other during the evolution.

Co-evolution of multi-sites in COVID-19 population

The strong co-occurrence relationships of multi-sites in COVID-19 virus suggested co-mutational evolution. We then investigated the co-occurrences of three groups involving 14 sites on a time scale of about per ten days. As shown in Fig. 3A, the mutation rates of the first group containing 6 sites exhibited very similar trends. Strikingly, 4 mutant sites (S_23403, NSP12_14408, 5'UTR_241, and NSP3_3037) almost shared a same mutation rate curve. A second group involved 5 sites (ORF8_28144, NSP4_8782, NSP14_18060, NSP13_17858, and NSP13_17747) and two mutant sites (ORF8_28144 and NSP4_8782) shared a same mutation rate curve whereas the other three mutant sites (NSP14_18060, NSP13_17858, and NSP13_17747) almost had a same mutation rate curve (Fig. 3B). We analyzed the correlations of the 11 mutant sites of the first and the second groups on a 15 intervals by Pearson Correlation Coefficient (PCC) (*20-22*), and expressed them by heatmap (Fig. 3C). There were two red (6*6 and 5*5) regions that corresponded to the first and the second mutant groups, respectively. As expected, the top 5 mutation sites, especially the top 4 sites in the first group exhibited a very strong correlation. In the second red (5*5) region corresponded to the second group, there were two subgroups containing a two-site (ORF8_28144 and NSP4_8782) and a triple-site (NSP14_18060, NSP13_17858 and NSP13_17747) exhibited very strong correlations, respectively (Fig. 3C).

Unlike the first and the second groups, the third group consisted of three *adjacent* mutation sites in nucleocapsid region (N_28881, N_28882, and N_28883). The mutation rate curve of these sites almost overlapped with each other and the mutation rates of these sites increased over time (Fig. 3D). The correlations of these sites were nearly 1.0 (Fig. 3D), suggesting a strong co-evolution.

Based on the relationships of the top two multi-site mutation groups, we illustrated the correlation networks of these mutations. As shown in Fig. 3E, the correlation networks of the first group mutation sites showed a six-pointed star and that of the second group showed a five-pointed star network. The mutation sites exhibited strong correlations with each other (Fig. 3E) and the correlations were further evidenced by the heatmap as show in Fig. 3F.

The mutations either changed the amino acid sequence or not. The mutation NSP2_c-1059-t resulted in an amino acid change (T85I) in the NSP2; the mutation NSP12_c-14408-t resulted in an amino acid change in the viral RNA-dependent RNA polymerase NSP12 (P323L) (fig. S1); the mutation S_a-23403-g resulted in an amino acid change in Spike protein (S)(D614G), which enhances viral infectivity (*6, 16*); the mutation ORF3a_g-25563-t resulted in an amino acid change (Q57H) in Spike protein in ORF3a; the mutation NSP13_c-17747-t and NSP13_a-17858-g resulted

154 in an amino acid changes P504L and Y541C in the NTPase/helicase domain NSP13, respectively;
155 the mutation ORF8_t-28144-c resulted in an amino acid change (L84S) in the ORF8; the mutations
156 N_g-28881-a, N_g-28882-a, N_g-28883-c resulted amino acid changes R203K, R203S and G203R
157 in the nucleocapsid N, respectively (Fig. 3G). In contrast, the mutations NSP14_c-18060-t and
158 NSP3_c-3037-t were synonymous mutations without amino acid changes (Fig. 3G). The mutation
159 5'UTR_c-241-t located in the 5'-non-translated region and did not change the predicted RNA
160 structure of 5'UTR (fig. S2).

161 **Significant decrease of CpG dinucleotide content in 5'UTR in COVID-19 population over time**

162 The CpG content of viral genome is restricted by host intrinsic zinc finger antiviral protein that
163 interacts with CpG rich-region and mediates depletion of foreign viral RNAs (*14, 23*). Comparing
164 with other coronaviruses, SARS-CoV-2 genome exhibits extreme CpG deficiency (*13*). However, the
165 evolutional trajectory of SARS-CoV-2 CpG-content within the same species is still unclear. We
166 investigated the CpG-content changes in SARS-CoV-2 since the outbreak. As shown in Fig. 4A and
167 4B, the CpG dinucleotide content exhibited a decreased trend over time. The CpG-content in each
168 SARS-CoV-2 genome regions varied, with high CpG-contents the 5'UTR, NSP1, E and ORF10
169 regions and low CpG-contents in NSP8, ORF6 regions. Notably, the NSP7 region was free of CpG
170 dinucleotide (Fig. 4C). Comparing with the first posted SARS-CoV-2 genome (NC_045512), in the
171 very recent SARS-CoV-2 genomes, only the CpG-contents of 5'UTR decreased significantly but not
172 the other CpG high content regions NSP1, E and ORF10 (Fig. 4D, E), suggesting a biased evolution
173 pressure on this region.

174 # CONCLUSION

175 Our comprehensive and massive mutation and correlation analyses identified four dominant
176 mutation sites (5'UTR_c-241-t, NSP3_c-3037-t, NSP12_c-14408-t, and S_a-23403-g) and revealed
177 three significant multi-site co-mutational patterns (S_a-23403-g, NSP12_c-14408-t, 5'UTR_c-241-t,
178 NSP3_c-3037-t, ORF3a_c-25563-t; ORF8_t-28144-c, NSP4_c-8782-t, NSP14_c-18060-t,
179 NSP13_a-17858-g, NSP13_c-17747-t; and N_g-28881-a, N_g-28882-a, N_g-28883-c). Some of the
180 mutations changed the amino acid sequence in the viral RNA-dependent RNA polymerase nsp12
181 (P323L), Spike protein (S) (D614G), ORF3a (Q57H), NTPase/helicase domain nsp13 (P504L,
182 Y541C), ORF8 (L84S) and nucleocapsid N (R203K, R203S, G203R), or did not change the amino
183 acid sequence (NSP14_c-18060-t and NSP3_c-3037-t), which may affect viral replication or
184 virus-host interaction. Other mutations were synonymous mutations without amino acid changes (Fig.

3G). And mutations located in the 5'-non-translated region (5'UTR_c-241-t) that did not change the predicted RNA structure. Moreover, we found gradual but significant decrease of CpG-content in 5'UTR region over time, which suggested the 5'UTR region as a potential ZAP target. Taken together, our study provides valuable clues and frameworks to dissect the viral replication and virus-host interactions for designing effective therapeutics.

Acknowledgments: We thank associate prof. T.Z. and Dr. S.T.H. for useful comments on the manuscript.

Funding: This work is supported by the National Key Research and Development Program of China (2017YFA0505500 to L.N.C., 2017YFC0909502 to J.S.Z.); the Strategic Priority Research Program of the Chinese Academy of Sciences (XDB38040400 to L.N.C.); National Science Foundation of China (31771476 and 31930022 to L.N.C, 61602460 and 11701379 to J.S.Z.); Shanghai Municipal Science and Technology Major Project (2017SHZDZX01 to L.N.C.); National Science and Technology Major Project of China (2017ZX10103009 to Z.G.Y.); Emergency Project of Shanghai Science and Technology Committee (20411950103 to Z.G.Y.); Development programs for COVID-19 of Shanghai Science and Technology Commission (20431900401 to Z.G.Y.); National Postdoctoral Program for Innovative Talent (BX20180331 to J.Y.K.); and China Postdoctoral Science Foundation (2018M642018 to J.Y.K.).

Author contributions: L.N.C. and J.S.Z. designed the study. J.S.Z. and Z.G.Y. designed the experiments. J.S.Z. analyzed data. J.S.Z., Z.G.Y., and J.Y.K. designed the figures. H.B.H. checked the experiments. J.S.Z. wrote the manuscript. Z.G.Y., J.Y.K., M.F.L., L.L., and Y.Q.H polished the manuscript.

Data and materials availability: All data are available in the main text or supplementary materials or from the corresponding author upon request.

Conflict of interest

The authors declare no conflict of interest.

Supplementary Materials:

Figs. S1 and S2

References and Notes:

1. D. Wrapp *et al.*, Cryo-EM structure of the 2019-nCoV spike in the prefusion conformation. *Science* **367**, 1260-1263 (2020).
2. M. Chinazzi *et al.*, The effect of travel restrictions on the spread of the 2019 novel coronavirus (COVID-19)

outbreak. *Science*, 395-400 (2020).

3. N. Zhu *et al.*, A Novel Coronavirus from Patients with Pneumonia in China, 2019. *The New England journal of medicine* **382**, 727-733 (2020).
4. P. Zhou *et al.*, A pneumonia outbreak associated with a new coronavirus of probable bat origin. *Nature* **579**, 270-273 (2020).
5. L. Chen *et al.*, RNA based mNGS approach identifies a novel human coronavirus from two individual pneumonia cases in 2019 Wuhan outbreak. *Emerging microbes & infections* **9**, 313-319 (2020).
6. B. Korber *et al.*, Tracking changes in SARS-CoV-2 Spike: evidence that D614G increases infectivity of the COVID-19 virus. *Cell*, (2020).
7. E. C. Smith, H. Blanc, M. Vignuzzi, M. R. Denison, Coronaviruses Lacking Exoribonuclease Activity Are Susceptible to Lethal Mutagenesis: Evidence for Proofreading and Potential Therapeutics. *Plos Pathog* **9**, (2013).
8. M. Sevajol, L. Subissi, E. Decroly, B. Canard, I. Imbert, Insights into RNA synthesis, capping, and proofreading mechanisms of SARS-coronavirus. *Virus Res* **194**, 90-99 (2014).
9. M. Vignuzzi, J. K. Stone, J. J. Arnold, C. E. Cameron, R. J. N. Andino, Quasispecies diversity determines pathogenesis through cooperative interactions in a viral population. **439**, 344-348 (2006).
10. N. D. Grubaugh, W. P. Hanage, A. L. Rasmussen, Making sense of mutation: what D614G means for the COVID-19 pandemic remains unclear. *Cell*, (2020).
11. B. A. *et al.*, Antibody cocktail to SARS-CoV-2 spike protein prevents rapid mutational escape seen with individual antibodies. *Science*, (2020).
12. J. Hansen *et al.*, Studies in humanized mice and convalescent humans yield a SARS-CoV-2 antibody cocktail. *Science*, (2020).
13. X. Xia, Extreme Genomic CpG Deficiency in SARS-CoV-2 and Evasion of Host Antiviral Defense. *Molecular Biology and Evolution*, (2020).
14. J. L. Meagher *et al.*, Structure of the zinc-finger antiviral protein in complex with RNA reveals a mechanism for selective targeting of CG-rich viral sequences. *P Natl Acad Sci USA* **116**, 24303-24309 (2019).
15. M. Ficarelli *et al.*, KHNYN is essential for the zinc finger antiviral protein (ZAP) to restrict HIV-1 containing clustered CpG dinucleotides. *Elife* **8**, (2019).
16. Q. Li *et al.*, The impact of mutations in SARS-CoV-2 spike on viral infectivity and antigenicity. *Cell*, (2020).
17. J. S. Zhang, Y. L. Wang, C. Zhang, Y. Y. Shi, Mining Contiguous Sequential Generators in Biological Sequences. *Ieee Acm T Comput Bi* **13**, 855-867 (2016).
18. J. S. Zhang, Y. L. Wang, D. Y. Yang, CCSpan: Mining closed contiguous sequential patterns. *Knowl-Based Syst* **89**, 1-13 (2015).
19. J. S. Zhang *et al.*, Efficient Mining Multi-Mers in a Variety of Biological Sequences. *Ieee Acm T Comput Bi* **17**, 949-958 (2020).
20. W. Wiedermann, M. Hagmann, Asymmetric properties of the Pearson correlation coefficient: Correlation as the negative association between linear regression residuals. *Commun Stat-Theor M* **45**, 6263-6283 (2016).
21. Y. S. Mu, X. D. Liu, L. D. Wang, A Pearson's correlation coefficient based decision tree and its parallel implementation. *Inform Sciences* **435**, 40-58 (2018).
22. G. Y. Mao, On high-dimensional tests for mutual independence based on Pearson's correlation coefficient. *Commun Stat-Theor M* **49**, 3572-3584 (2020).
23. V. Odon *et al.*, The role of ZAP and OAS3/RNAseL pathways in the attenuation of an RNA virus with elevated frequencies of CpG and UpA dinucleotides. *Nucleic Acids Res* **47**, 8061-8083 (2019).

Figure 1

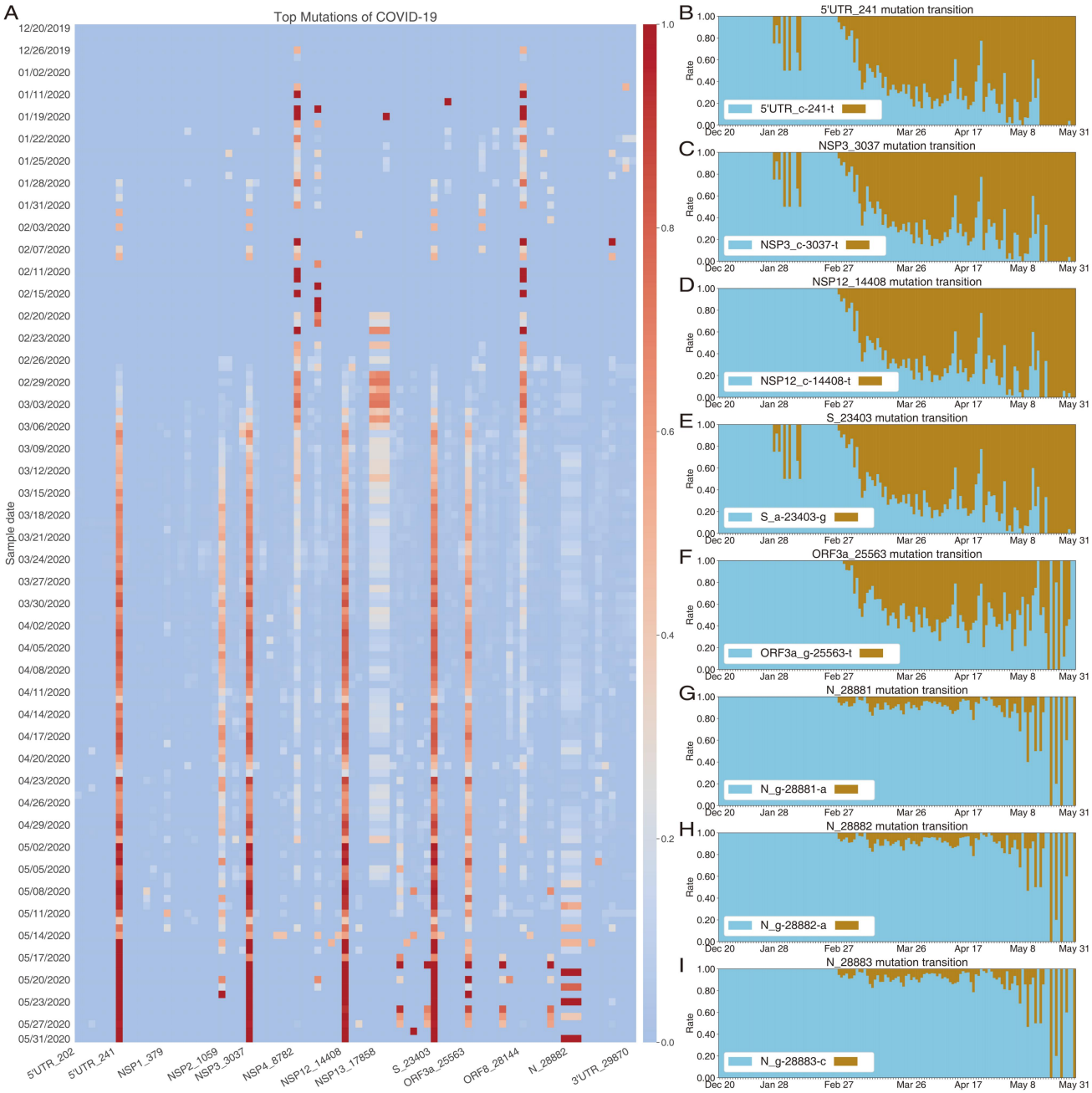

Fig. 1. Ongoing and dominant mutations of SARS-CoV-2 over time. (A) The global mutational landscape of top 1% mutation rates from Dec. 20, 2019 to May 31, 2020. The mutation of SARS-CoV-2 is clearly ongoing and yet with a rapid rate. **(B)- (I)** show the mutation transitions of 8 sites from Dec. 20, 2019 to May 31, 2020. The sky-blue represents the rates of the original nucleic acids in reference sequence, and the dark-golden the rates of the mutant nucleic acids. Note that the 5 mutations (subfigures B to F), i.e., 5'UTR_c-241-t, NSP3_c-3037-t, NSP12_c-14408-t, and S_a-23403-g, and ORF3a_c-25563-t, especially the top 4 ones have clearly become the dominant mutants. The three adjacent mutations (subfigures G to I, N_ g-28881-a, N_ g-28882-a, and N_g-28883-c) increase daily on the whole.

Figure 2

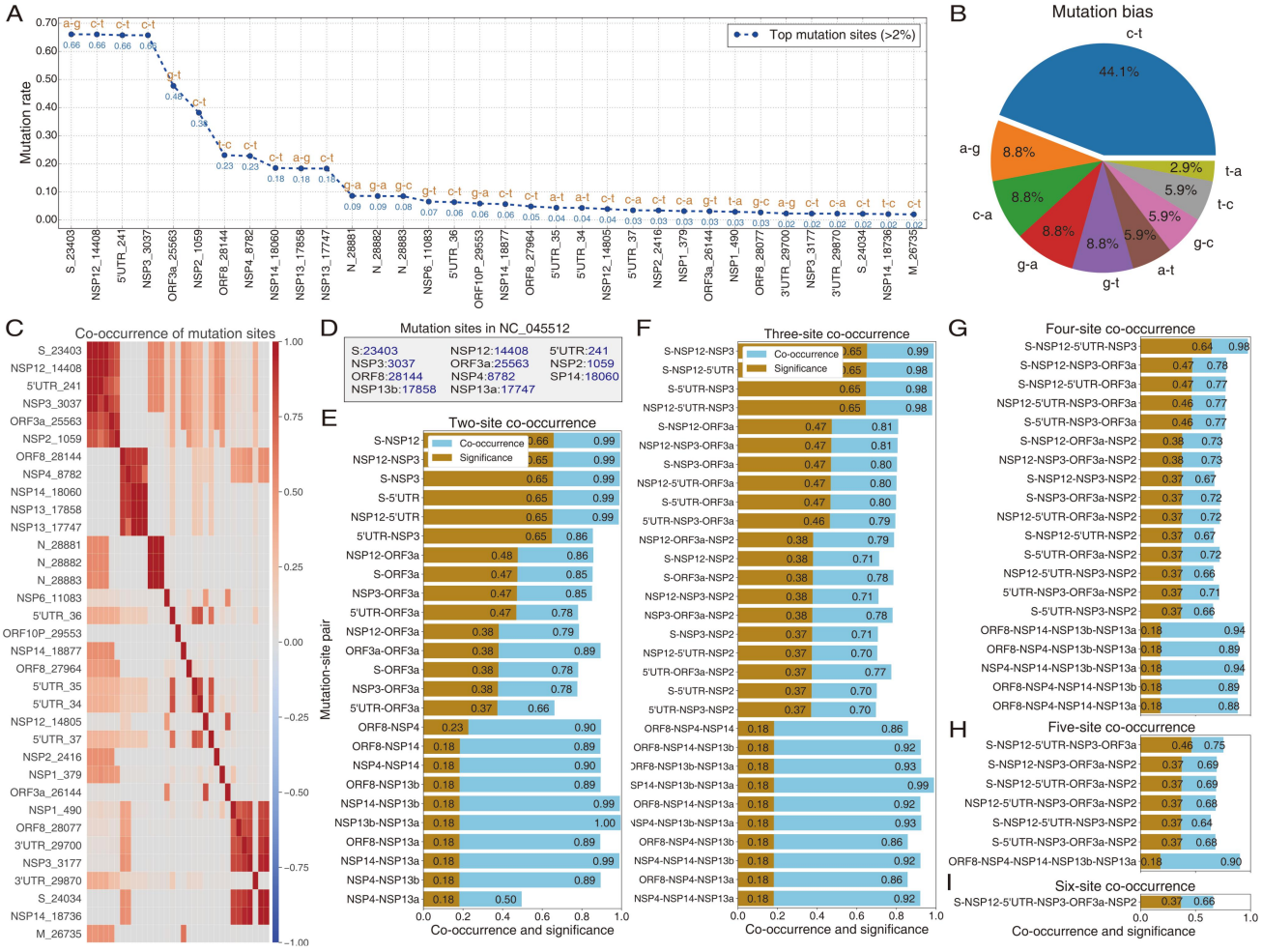

Fig. 2. Co-ocurrence mutations of SARS-CoV-2 over time. (A) Top 2% mutation sites involve 34 sties. The top 11 sites hold significant high mutation rates. **(B)** Mutation bias of the top 34 mutants. **(C)** Co-occurrence heatmap of top 2% mutation sites in order of mutational significance. The X-axis and Y-axis share the same tick labels (mutation sites along with their positions in reference sequence NC_045512) as shown in Y-axis. The top 14 sites were clustered into three high co-occurrence groups. **(D)** Query table of top 11 mutation sites. We used gene names instead of their mutation sites in subfigures (E) to (I), for simplicity. **(E)** Co-occurrences of 2 mutation sites. Each tick label of Y-axis, like S-NSP12, represents the mutation-site association/pattern of gene S (position 23403) and NSP12 (position 14408). The detailed positions of these mutations are shown in subfigures (E). **(F)** Co-occurrences of 3 mutation sites. **(G)** Co-occurrences of 4 mutation sites. **(H)** Co-occurrences of 5 mutation sites. **(I)** Co-occurrences of 6 mutation sites.

288 **Figure 3**

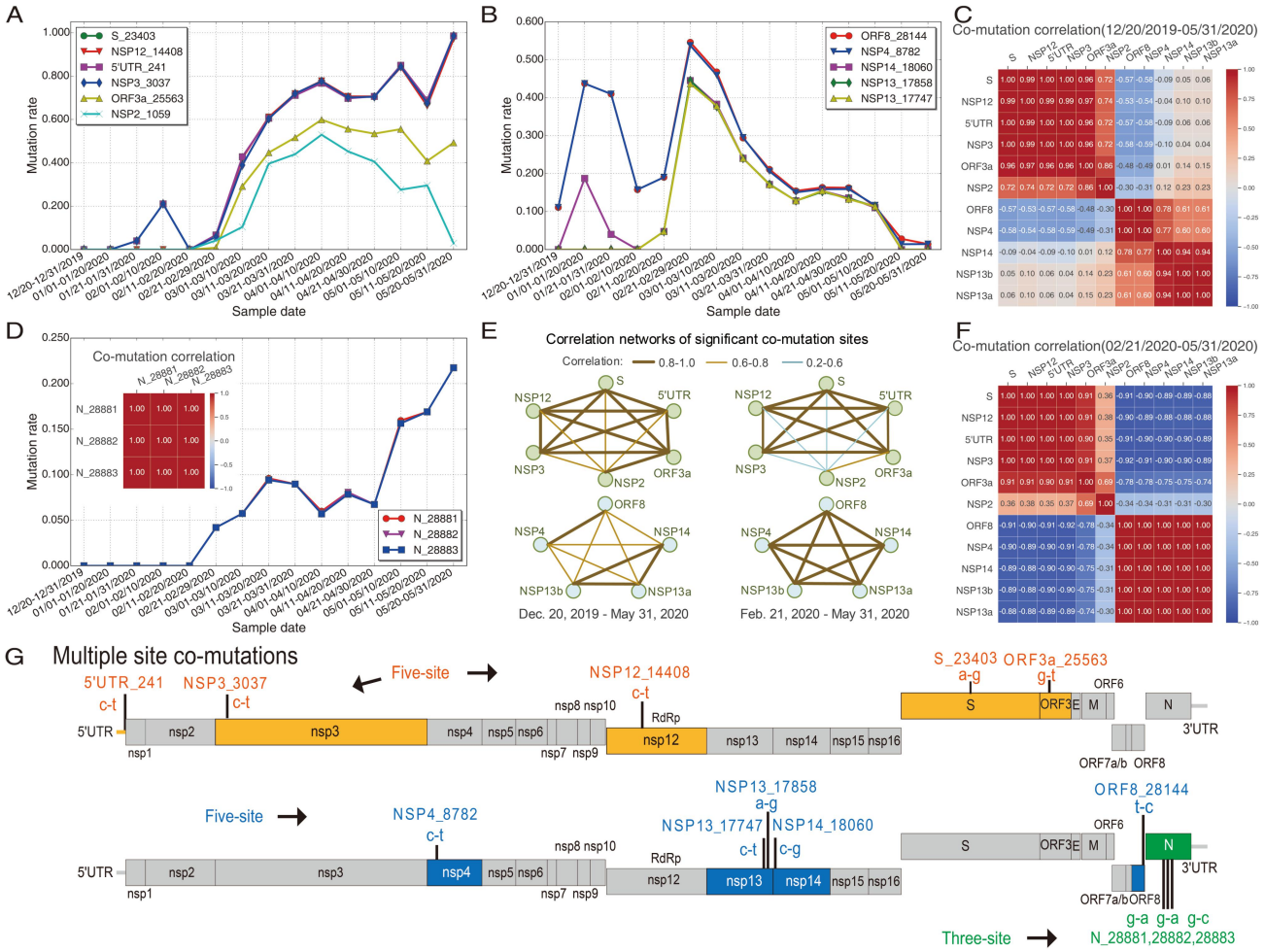

289

290 **Fig. 3. Co-evolution of multi-sites in COVID-19 population over time. (A)** Mutation trends of top
291 6 sites in Fig. 2A from Dec. 20, 2019 to May 31, 2020. **(B)** Mutation trends from the 7th to 11th sites
292 in Fig. 2A. **(C)** Global co-mutational heatmap of top 11 in Fig. 2A sites since Dec. 20, 2019. **(D)**
293 Mutation trends and co-mutational heatmap of three adjacent Nucleocapsid sites (from 12th to 14th
294 sites in Fig.2A). **(E)** Correlation networks of significant co-mutation sites. The left two sites show
295 the correlation relationships from Dec. 20, 2019 to May 31, 2020, and the right two from Feb. 21,
296 2020 to May 31, 2020. **(F)** Co-mutational heatmap of top 11 sites with sample collection dates from
297 Feb. 21, 2020 to May 31, 2020. **(G)** The mutational positions of multi-site co-mutations consisting of
298 5-, 5- and 3-site co-mutations.

299
300
301
302
303
304
305
306

Figure 4

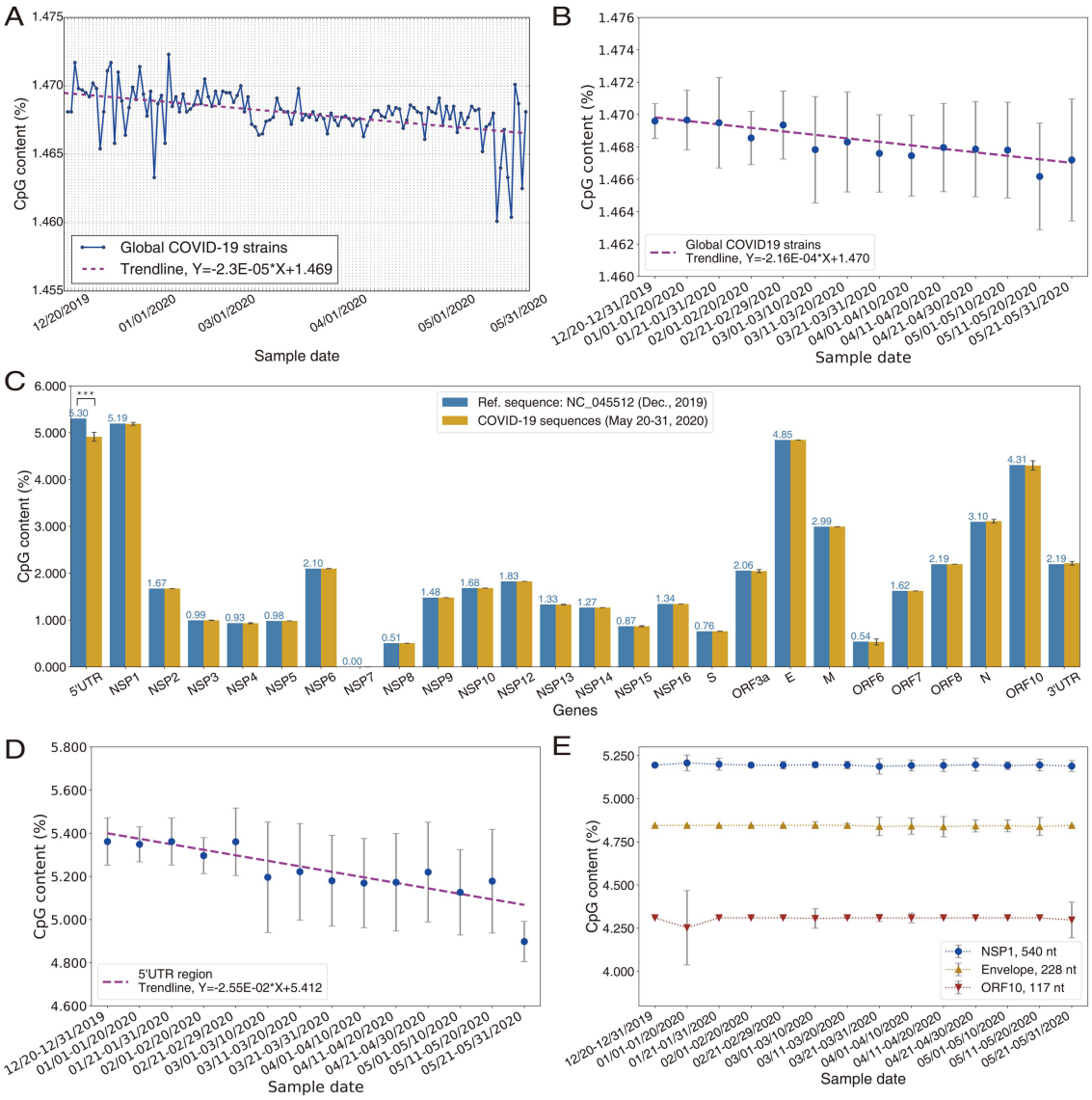

Fig. 4. CpG-content decrease in COVID-19 population over time. (A) Trend of CpG decrease of COVID-19 genome per day. **(B)** Trend of CpG decrease of COVID-19 genome by intervals of about 10 days. **(C)** CpG changes of all genes. The significant decrease of only 5'UTR region indicates that 5'UTR is the potential target gene of ZAP. **(D)** Trend of CpG decrease of 5'UTR region by about 10 days.` **(E)** CpG change trends of NSP1, Envelope, and ORF10.